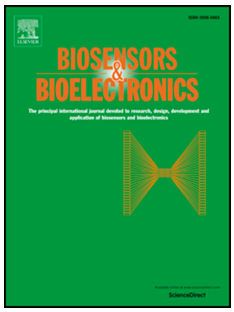

Rational design of electroactive redox enzyme nanocapsules for high-performance biosensors and enzymatic biofuel cell

Jie Huang, Yuxuan Zhang, Fei Ding, Dong Chen, Yiwen Wang, Xin Jin, Xinyuan Zhu

PII: S0956-5663(20)30792-2

DOI: https://doi.org/10.1016/j.bios.2020.112805

Reference: BIOS 112805

To appear in: *Biosensors and Bioelectronics*

Received Date: 23 September 2020

Revised Date: 4 November 2020

Accepted Date: 5 November 2020

Please cite this article as: Huang, J., Zhang, Y., Ding, F., Chen, D., Wang, Y., Jin, X., Zhu, X., Rational design of electroactive redox enzyme nanocapsules for high-performance biosensors and enzymatic biofuel cell, *Biosensors and Bioelectronics* (2020), doi: https://doi.org/10.1016/j.bios.2020.112805.

CRediT authorship contribution statement

Jie Huang: Data curation, Methodology, Visualization, Formal analysis, Writing - original draft.

Yuxuan Zhang: Data curation.

Fei Ding: Writing - review & editing.

Dong Chen: Methodology.

Yiwen Wang: Writing - review & editing.

Xin Jin: Conceptualization, Methodology, Writing - review & editing, Funding acquisition, Project administration.

Xinyuan Zhu: Supervision, Project administration, Funding acquisition.

Rational design of electroactive redox enzyme nanocapsules for high-performance biosensors and enzymatic biofuel cell

Jie Huang, Yuxuan Zhang, Fei Ding, Dong Chen, Yiwen Wang, Xin Jin, * Xinyuan Zhu

School of Chemistry and Chemical Engineering, S

tate Key Laboratory of Metal Matrix Composites, Shanghai Jiao Tong University, 800 Dongchuan Road, Shanghai 200240, PR China

∗ Corresponding authors.

E-mail addresses: jxcindy@sjtu.edu.cn (X. Jin)

Abstract

The potential application of biodevices based on enzymatic bioelectrocatalysis are limited by poor stability and electrochemical performance. To solve the limitation, modifying enzyme with functional polymer to tailor enzyme function is highly desirable. Herein, glucose oxidase (GOx) was chosen as a model enzyme, and according to the chemical structure of GOx cofactor (flavin adenine dinucleotide, FAD), we customize a biomimetic cofactor containing vinyl group (SFAD) for GOx, and prepared an GOx nanocapsule via in-situ polymerization. The characterization of particle size distribution, TEM, fluorescence and electrochemical performance indicated the successful formation of electroactive GOx nanocapsule with SFAD-containing polymeric network(n(GOx-SFAD-PAM)). The network can act as an electronic “highway” to link the active site with electrode, with capability to accelerate electron transfer as well as enhanced GOx stability. Further investigation of bioelectrocatalysis shows that n(GOx-SFAD-PAM)-based biosensor has low detection

potential (-0.4 vs. Ag/AgCl), high sensitivity (64.97 $\mu AmM^{-1}cm^{-2}$), good anti-interference performance, quick response (3□5s) and excellent stability, and that n(GOx-SFAD-PAM)-based enzymatic biofuel cell (EBFC) has the high maximum power density (1011.21 μWcm^{-2}), which is a 386-fold increase over that of native GOx-based EBFC (2.62 μWcm^{-2}). This study suggests that novel enzyme nanocapsule with electroactive polymeric shell might provide a prospective solution for the performance improvement of enzymatic bioelectrocatalysis-based biodevices.

Keywords: glucose oxidase; biomimetic cofactor; enzyme modification; enzyme nanocapsule; glucose biosensor; enzymatic biofuel cells

1. Introduction

During the evolution of nature, a series of impressive redox enzymes was evolved through natural selection, for catalyzing redox reactions(Caruana and Howorka, 2010; Güven et al., 2010; Wong and Schwaneberg, 2003). Redox enzymes are also widely used as powerful biocatalysts to build enzymatic biosensors(B et al., 2020; Chen et al., 2011; Dhanjai et al., 2020; Wu et al., 2018) and EBFCs(Kang et al., 2019; Mahadevan et al., 2016; Yin et al., 2019), undergoing a bioelectrocatalysis process(Chen et al., 2020; Karyakin et al., 2007; Ruff et al., 2020). The natural structure of redox enzymes is revolutionized to react as catalyst in specific natural circumstances, but not to react as biocatalyst in electrochemical conditions. Generally, their active site (active center) is embedded in protective protein shells, which is its natural advantage to keep specific and stable catalysis condition but nearly chemically insulated(Campbell et al., 2016; Nicolas and Mano, 2019; Wu et al., 2017). In

bioelectrocatalysis, however, such protein shell greatly attenuates the electron transfer between the active site and electrodes, leading to a disadvantage for efficiency(Adrian et al., 2018; Cheong et al., 2018; Xiao et al., 2019). Other problems might also need to be fixed, such as how to protect the spatial structure of natural redox enzyme, and how to maintain their catalytic properties in bioelectrocatalysis circumstances(B et al., 2020; Dhanjai et al., 2020; Moehlenbrock and Minteer, 2008; Zhang et al., 2017a). These problems bring a series of troubles in bioelectrocatalysis applications, such as low sensitivity, slow response and poor stability of enzymatic biosensors (Deng et al., 2014; Ruzgas et al., 2007; Wei et al., 2018), as well as low power output(Chen et al., 2015; Huang et al., 2019; Ji et al., 2017) and short life(Boussema et al., 2018; Panpan et al., 2015; Yan et al., 2006) of EBFCs.

In the last two decades, to solve these problems, researchers have been working on constructing an efficient electron transmission interface between redox enzyme and the electrode surface(Scherbahn et al., 2014; Song et al., 2019; Wang et al., 2020). The main strategy of interfaces design is the integration of nanomaterials to modify the electrode to improve the electron transfer ability(Feng et al., 2010; Gao et al., 2010; Han et al., 2015; Zhang et al., 2016). With the development of nanomaterials, the performance of nanomaterial-based EBFCs have been greatly improved(Gao and Duan, 2015; Jin-Zhong et al., 2003; Qu et al., 2017; Zhao et al., 2017). However, due to the defects of the natural redox enzyme, EBFCs still cannot meet the requirements of application(Jeerapan and Ma, 2019; Rasmussen et al., 2016). Therefore, more and more researchers began to pay attention to the enzyme modification to further

enhance the performance of enzymatic bioelectrocatalysis devices(Caruana and Howorka, 2010; Güven et al., 2010; Wong and Schwaneberg, 2003). Enzyme modification was realized through protein engineering, such as chemical modification(Dong et al., 2018; Minteer et al., 2015; Murata et al., 2013; Szczesny et al., 2020), rational design(Courjean et al., 2010; Demin and Hall, 2009), directed evolution(Arnold and H, 2018; Arnold, 2018; Ma et al., 2020; Schwaneberg et al., 2019) and other combined methods. For example, hypoglycosylation of enzyme has been proved with improved electrochemical performance but poor thermostability(Courjean et al., 2010), while hyperglycosylation strategy usually obtains improved stability and probably poor electrochemical properties(Nicolas and Mano, 2019). A novel strategy obtaining both electrochemical and stability properties is highly desired.

In order to prepare high-performance biosensors and enzymatic biofuel cell, herein we report a rational design of electroactive redox enzyme nanocapsule with mediator-containing polymeric network, through in situ polymerization(Cal et al., 2014; Zhang et al., 2017c; Zhang et al., 2018). In obtained nanocapsule, the polymeric network acts as an electronic “highway” to link the active site with electrode, with capability to accelerate electron transfer between them. To successfully prepare efficient enzyme nanocapsules, two key points are considered in the design. Firstly, such mediator should have similar structure as cofactor to guarantee a similar redox potential, which benefits to the electron transfer between cofactor and the network(Kazarinov et al., 2014; Masuda et al., 2010; Nicolas and Mano, 2019).

Secondly, it is better to introduce polymerizable vinyl group to mediator, in order to prepare enzyme nanocapsule through in situ polymerization, which has been proven as a perfect method to maintain GOx activity as much as possible with enhanced GOx stability(Li et al., 2015; Wei et al., 2013).

Based on the key points above, we herein selected GOx as a model redox enzyme to prepare an efficient GOx nanocapsule because GOx is notoriously difficult to achieve direct electron transfer between the FAD and the electrode. As illustrated in **Scheme 1**, GOx nanocapsule containing electron relay network is constructed via three steps:

Step 1) we refer to chemical structure of the FAD, and designed and chemically synthesized a biomimetic cofactor monomer containing vinyl group (SFAD);

Step 2) the polymerizable GOx was generated by the reaction between acrylic acid N-hydroxylsuccinimide ester (NAS) and amino group of GOx;

Step 3) the polymerizable GOx reacted with SFAD and other monomers via situ polymerization to form electroactive GOx nanocapsule;

According to our previous work(Dong et al., 2018; Zhang et al., 2017b; Zhang et al., 2017c), the GOx nanocapsule prepared via in-situ polymerization can enhance stability even at harsh conditions because of the polymeric network. Importantly, SFAD, as a hydrophobic monomer, tends to polymerize in the cavity of GOx, and thus promote an effective wiring of the GOx active site to electrode(Huang J and Yiwen Wang, 2020).

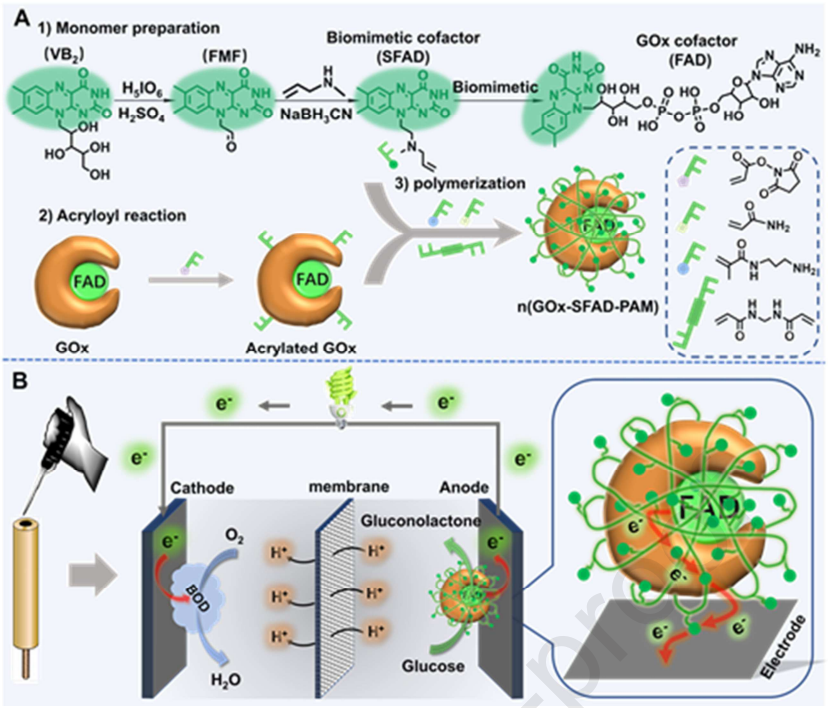

Scheme 1. A, B) Schematics of SFAD synthesis, and the preparation of n(GOx-SFAD-PAM) nanocapsules (A) and their Mechanism for bioelectrocatalysis (B).

2. Experimental

Full details about the preparation of GOx nanocapsules, the construction of GOx nanocapsule-based biosensor and EBFC, and electrochemical testing has been given in the Supporting Information.

3. Results and discussion

3.1. Preparation and characterization of GOx nanocapsules

Detailed process of preparing GOx nanocapsule is as follows: side chain on the 2′-C site of Vitamin B2 is firstly oxidized into aldehyde group in the action of periodic acid and sulfuric acid to obtain FMF(Sakai et al., 2018). Then the aldehyde group on the product was reacted with the secondary amine group of N-Methylallylamine (NMAA) to form Schiff base with a followed reductive

amination using mild reductant $NaBH_3CN$ to obtain SFAD. The products involved in each step are characterized by nuclear magnetic resonance (NMR) spectroscopy (Supporting Information, **Figures S1, S2, S4, S5**) and Mass spectrometry (MS) (Supporting Information, **Figure S3, S6**), which verified the successful syntheses of FMF and SFAD. In addition, the redox potential of SFAD is close to that of FAD reported in the literature(Kang et al., 2018), and the results are shown in **Figure S7**. After the synthesis of SFAD, the native GOx was reacted with the N-acryloxysuccinimide (NAS) at predetermined molar ratio (native GOx/NAS = 1:50) in 0.02M PBS (pH 8.0). After the reaction was over, the excessive NAS was removed to get the acryloylated GOx, which was furtherly characterized by MALDI-TOF-MS. The results show that there were an average of twelve acrylamide moieties on the surface of acryloylated GOx (**Figure 1A**). The obtained acryloylated GOx reacted with SFAD, acrylamide (AAm), (N-(3-aminopropyl) methacrylamide (APM) and the crosslinker (N, N′-methylenebisacrylamide) (BIS) by in situ polymerization method to form the GOx nanocapsule, n(GOx-SFAD-PAM). Similarly, nanocapsule without SFAD is called n(GOx- PAM). The molar ratio of monomers (AAm, APM, SFAD and BIS) were listed in **Table S1**. Polymerization was initiated by the addition of ammonium persulfate (APS) and N,N,N′,N′-tetramethyl-ethylene diamine (TEMED). As shown in the **Figure 1B,** the native GOx shows a size distribution centered at 8 nm, the result is similar to those that have been well documented(Dong et al., 2018). For comparison, the size distribution centered of n(GOx-SFAD-PAM) is 35 nm, suggesting that a polymer network successfully form around the enzyme surface. As

shown in **Figure S8,** spherical nanocapsules with uniform distribution obtained from TEM images, and the TEM results are consistent with the DLS results. According to the results (**Figure 1C**), native GOx and n(GOx-SFAD-PAM) have similar fluorescence emission wavelength. It is mainly due to the similar chemical structure of FAD and SFAD. However, native GOx shows weak fluorescence intensity because FAD is deeply embedded in protein shell. In contrast, SFAD is distributed on the periphery of active site, not restricted by protein shell coating, so it shows a significant fluorescent intensity(Dong et al., 2018). Therefore, the significant increase of the fluorescence intensity can prove that SFAD has been successfully introduced into n(GOx-SFAD-PAM) and it can freely tumble in the nanocapsule. Considering the results from DLS, TEM, and fluorescence property collectively, GOx nanocapsule containing SFAD was successfully prepared.

The stability is an important enzyme function for bioelectrocatalysis applications in various circumstances. Therefore, we conducted stability tests under different temperature and pH conditions, using native GOx as comparison. As shown in the **Figure 1 D-F**, n(GOx-SFAD-PAM) exhibits excellent thermal and pH stability. After heat treatments at 60, 70 and 80 °C, rapid declined catalytic activity was observed on native GOx, with completely denaturation at 80 °C. While n(GOx-SFAD-PAM) retained most activity at 60 and 70°C, retaining more than one third of activity at 80 °C (**Figure 1D**). Both enzymes displayed a maximum activity at pH 5.0. At pH 3.0, however, native one loss only retained 33.3% of activity, while n(GOx-SFAD-PAM) retained 70.3% (**Figure 1E**). Furthermore, the encapsulation also can enhance the

storage stability of enzyme. As presented in Figure **1F**, native enzyme was fully denatured after 30-day storage at room temperature, whereas n(GOx-SFAD-PAM) still maintained 90%. Native GOx is easily denatured from the unfolding of protein structure and releasing of FAD, while n(GOx-SFAD-PAM) can prevent such unfolding and releasing with protective polymeric network(Ramanavicius et al., 2012).

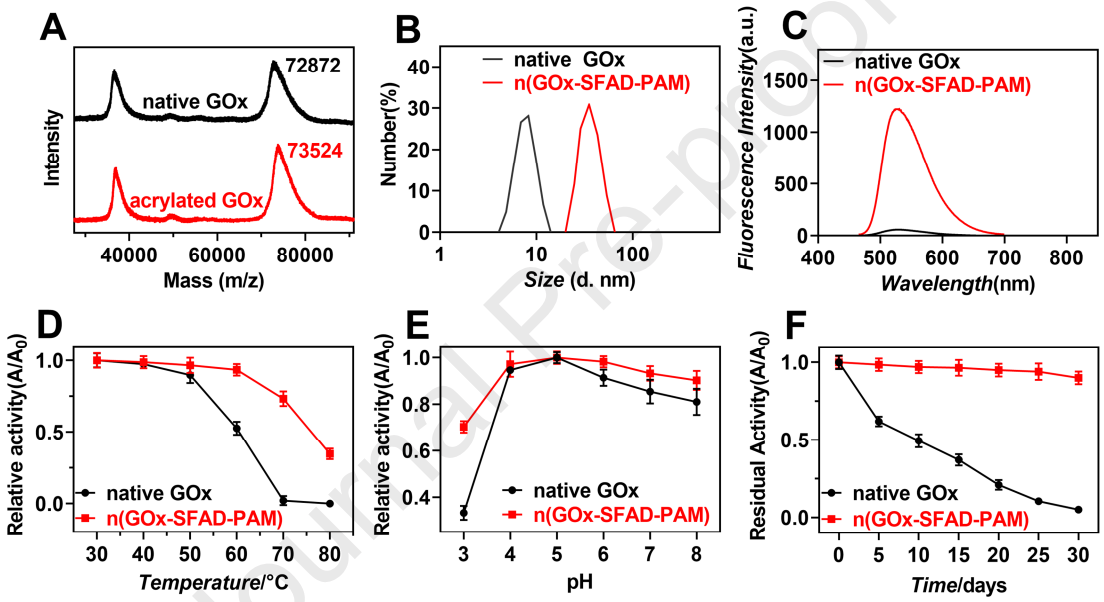

Figure 1. The formation and stability of n(GOx-SFAD-PAM) nanocapsules. A) MALDI-TOF mass spectroscopies of native GOx and acrylated GOx; B) Size distribution of native GOx and n(GOx-SFAD-PAM); C) Fluorescence spectrum of native GOx and n(GOx-SFAD-PAM); D) Thermo-stability comparison of native GOx and n(GOx-SFAD-PAM). The catalytic activity obtained at 30ºC was treated as 100%. E) pH stability comparison of native GOx and n(GOx-SFAD-PAM). The catalytic activity obtained at pH=5 was treated as 100%. F) Storage stability of native GOx and n(GOx-SFAD-PAM) at room temperature. The catalytic activity obtained on the first

day was treated as 100%. Data represent mean ± standard deviation (SD) from three independent experiments.

3.2. Characterization of enzyme-modified electrodes

For bioelectrochemical applications, uniform and stable conductive nanomaterials films with larger surface area should be generally needed to improve the efficient immobilization and utilization of biocatalysts. As shown in **Figure S9A**, compared with bare glassy carbon electrode (GCE) and graphene oxide (GO)/GCE, carboxyl Multi-walled carbon nanotube (cMWCNTs)/GCE has a larger response current. Moreover, cMWCNTs/GCE has the smallest *R*ct, as can be seen from **Figure. S9B**. These results indicate that cMWCNTs/GCE have better performance compared to GO/GCE. What is more, the cycle stability of the prepared cMWCNTs/GCE was detected by the CV for 50 cycles, as shown in **Figure S9C**. There was nearly no decay with the curves, indicating that cMWCNTs can be stably fixed on the surface of bare GCE. **Figure S9D** that there is an integrated free-standing three-dimensional network structure with well developed nanoscale pores at the cMWCNTs/GCE. The structure is beneficial to the efficient immobilization of biocatalysts. Therefore, we choose cMWCNTs/GCE to prepare the enzyme-modified electrode.

Next, enzyme-modified electrodes were prepared following reported method(Kang et al., 2018; Panpan et al., 2015) (detailed process in Supporting Information). Enzyme-modified electrodes using n(GOx-SFAD-PAM), native GOx and n(GOx-PAM) was denoted as n(GOx-SFAD-PAM)/cMWCNTs/GCE, native GOx/cMWCNTs/GCE and n(GOx-PAM)/ cMWCNTs/GCE, respectively. The

interaction between enzymes and cMWCNTs/GCE was investigated through cyclic voltammetry (CV). As shown in **Figure 2A**, there were no redox peak in CVs in either native GOx/cMWCNTs/GCE or n(GOx-PAM)/cMWCNTs/GCE, however a specific redox peak in n(GOx-SFAD-PAM)/cMWCNTs/GCE. Such results indicate that no direct electron transfer between electrode and native GOx or n(GOx-PAM), and prove a successful immobilization and electroactivity of n(GOx-SFAD-PAM). Next, surface characteristics of the three enzyme-modified electrodes were tested by electrochemical impedance spectroscopy (EIS) via using $[Fe(CN)_6]^{3-/4-}$ as a redox probe. In order to determine the corresponding electron transfer resistance (*Rct*), curves were fitted via equivalent circuit (**Figure. 2B** inset), and the results are shown in **Figure. 2B**. The diameter of this semicircular region of Nyquist plots represents *R*ct. Compared to *R*ct of cMWCNTs/GCE (**Figure S9**), *R*ct of native GOx/cMWCNTs/GCE, n(GOx-PAM)/cMWCNTs/GCE and n(GOx-SFAD-PAM)/cMWCNTs/GCE were greatly increased and the specific values were about 1960 Ω, 2330 Ω and 1070 Ω, respectively. This is because the protein shell impedes the redox probe's access to the electrode surface(Panpan et al., 2015). More importantly, the *R*ct of n(GOx-SFAD-PAM)/cMWCNTs/GCE is the smallest one in three enzyme-modified electrodes. As smaller *R*ct indicates a faster electron-transfer rate, our result proves that n(GOx-SFAD-PAM)/cMWCNTs/GCE is able to proceed a fast electron transfer, donated from the redox activity of polymeric network containing SFAD. Based on these data, our hypothesis is that SFAD might be able to improve the electron transfer between active site and electrode. Such

improvement is also proved through enzymatic catalytic kinetics data. As shown in **Figure 2C**, n(GOx-SFAD-PAM) behaved with increased k_{cat} than native GOx (from 763.72 ± 10.74 s^{-1} to 930.85 ± 24.20 s^{-1}). According to the catalytic mechanism of GOx (equation 1), a higher k_{cat} proves that SFAD can quickly obtain electrons from the reduced GOx ($FADH_2$) (equation 2) and accelerate the regeneration of the GOx, further proving an improved electron transfer in n(GOx-SFAD-PAM).

When glucose was added, a significantly increased oxidation peak current in CV was observed (**Figure 2D)**. The catalytic current produced, resulting from a sequence of electron-transfer, can be described by equations 1, equations 2 and equations 3. These results demonstrated that immobilized n(GOx-SFAD-PAM) maintain excellent catalytic activity and that the network containing SFAD could effectively shuttle electrons from the active site of GOx to the electrode. Combined with the reported literature(Krikstopaitis et al., 2004) and experimental results (**Figure S10**), we can infer that mediated electron transfer proceeded by intra- and intermolecular mechanism.

$$\boldsymbol{GOx(FAD) + glucose \rightarrow GOx(FADH_2) + gluconotone} \quad (1)$$

$$\boldsymbol{GOx(FADH_2) + SFAD \rightarrow GOx(FAD) + SFADH_2} \quad (2)$$

$$\boldsymbol{SFADH_2 + SFAD \leftrightarrow SFAD + SFADH_2} \quad (3)$$

The electrochemical properties of the n(GOx-SFAD-PAM)/cMWCNTs/GCE were evaluated via executing CVs at different scan rates. **Figure. S11A** shows the redox peak currents clearly increased with increasing potential scan rate. Moreover, the redox peak currents (I_{Pa} and I_{Pc}) were proportional to the scan rate *v*, proving that

the electrode reaction corresponds to a surface-controlled electrochemical process (**Figure. S11B)**. Then, the stability of the n(GOx-SFAD-PAM)/cMWCNTs/GCE was investigated, acting with little decrease of response current after 100 cycles **(Figure. S11C)**. Thanks to the high stability of n(GOx-SFAD-PAM), little decrease of response current was observed even after storage for 15 days (**Figure. S11D)**, indicating an excellent stability of n(GOx-SFAD-PAM)/cMWCNTs/GCE.

The excellent performance of n(GOx-SFAD-PAM)/cMWCNTs/GCE prompted us to apply it in biosensors and enzymatic biofuel cells. Based on the improved electron transfer and enhanced stability, we can expect that the n(GOx-SFAD-PAM)/cMWCNTs/GCE-based glucose biosensor has high sensitivity, good anti-interference performance, quick response and excellent stability, and that the n(GOx-SFAD-PAM)/cMWCNTs/GCE-based glucose/O_2 enzymatic biofuel cell has high output power and excellent stability.

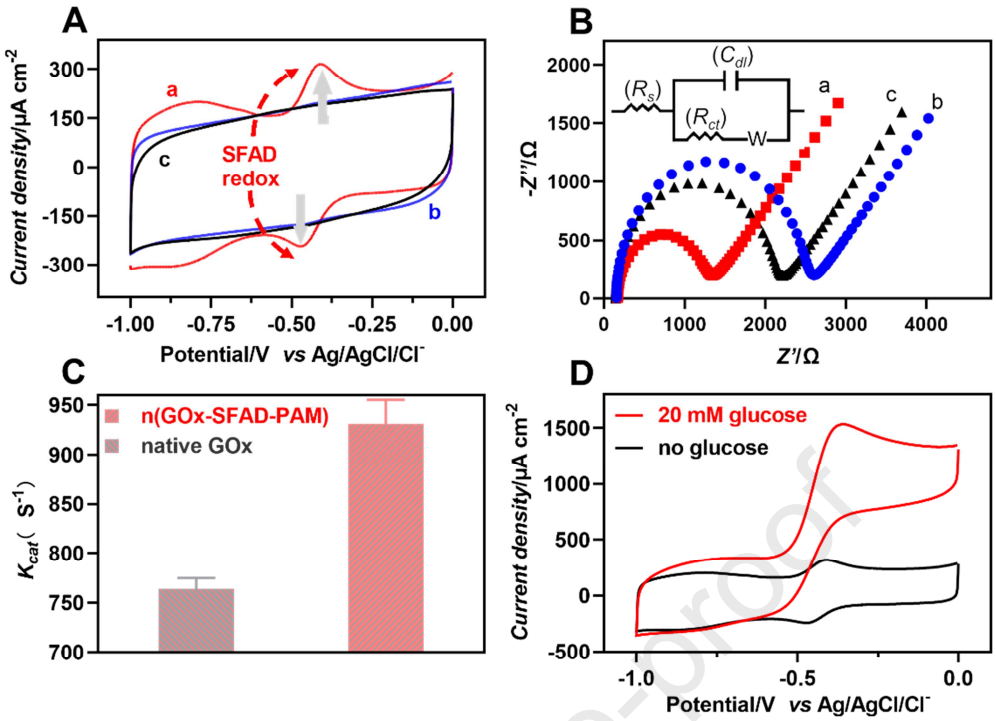

Figure 2. A) Cyclic voltammograms of n(GOx-SFAD-PAM)/cMWCNTs/GCE (a), n(GOx-PAM)/cMWCNTs/GCE (b), native GOx/cMWCNTs/GCE (c) in 0.1 M PBS (pH 7.4) saturated with N_2; **B)** Nyquist plots of electrochemical impedance spectra for n(GOx-SFAD-PAM)/cMWCNTs/GCE (a), n(GOx-PAM)/cMWCNTs/GCE (b) and native GOx/cMWCNTs/GCE (c) in 0.1M KCl with 1.0 mM $Fe(CN)_6^{3-/4-}$. Inset: equivalent circuit used to fit data, **C)** k_{cat} of native GOx and n(GOx-SFAD-PAM), **D)** Cyclic voltammograms of n(GOx-SFAD-PAM)/cMWCNTs/GCE in N_2- saturated 0.1 M PBS (pH 7.4) containing 0.02M glucose (a) or without glucose (b).

3.3. Characterization of n(GOx-SFAD-PAM)-based biosensor

The analytical performance of the biosensor was evaluated through the calibration curve. **Figure. S12** shows current-time response plot for the n(GOx-SFAD-PAM)-based biosensor, dealing with successive steps changes of glucose concentration at a relative low working potential of -0.4 V (vs. Ag/AgCl). The relationship between the electro-catalytic current and the concentration of the glucose was shown in **Figure. 3A**. The result demonstrates that

n(GOx-SFAD-PAM)/cMWCNTs/GCE-based biosensor has high sensitivity, and that detection range of the biosensor can be divided into two sections of 0.1–18 mM and 18–50 mM, both of them showing good linear fitness, with a sensitivity of 63.69 $\mu AmM^{-1}cm^{-2}$ and 12.23 $\mu AmM^{-1}cm^{-2}$, respectively. Blood glucose concentration of healthy people usually range from 4.4 to 6.6 Mm(Deng et al., 2014), and the Limit of Detection(LOD) of our biosensor was calculated to be 0.13 mM (**Figure. S12)**. Therefore, linear range of our biosensor is capable to meet quantify at the healthy blood glucose monitoring. The n(GOx-SFAD-PAM)/cMWCNTs/GCE-based biosensor also has quick response ability. After each addition of glucose, the response current can reach equilibrium in about 3-5s. This is owing to fast electron transfer donated by SFAD-containing polymeric network.

Moreover, anti-interference ability of biosensor was tested by adding some endogenous species (such as ascorbic acid (AA), dopamine (DA), and uric acid (UA)) during glucose analysis. As shown in **Figure. 3B**, 0.5 mM AA and 0.1 mM DA showed minor interference to the overall oxidation current, with 3.5% and 1.8% in 4 mM glucose, respectively. What's more, 0.5 mM UA hardly affects the glucose analysis. These results demonstrate a strong anti-interference performance for n(GOx-SFAD-PAM)/cMWCNTs/GCE-based biosensor, attributed from low redox potential of SFAD as well as low operating potential of biosensor(Deng et al., 2014). The n(GOx-SFAD-PAM)/cMWCNTs/GCE-based biosensor also exhibited excellent repeatability (five repeated measurements) with an average relative standard deviation of 2.15% (**Figure. 3C**). Storage stability of the

n(GOx-SFAD-PAM)/cMWCNTs/GCE-based biosensor was investigated by an everyday monitoring of its response current to 4 mM glucose. As shown in **Figure. 3D**, the biosensor maintained 97% of its response current even after 15 days' storage period. Moreover, we also applied our biosensor to determine the glucose concentration of real samples. The results, as listed in **Table S2**, indicate that the glucose biosensor have excellent accuracy, precision, and recovery, and that it is capable to test practical sample. The n(GOx-SFAD-PAM)/cMWCNTs/GCE-based glucose biosensor prepared in this study has more excellent overall performances than other reported biosensors, comparison data listed in **Table S3**, largely attributed to the rational design of n(GOx-SFAD-PAM).

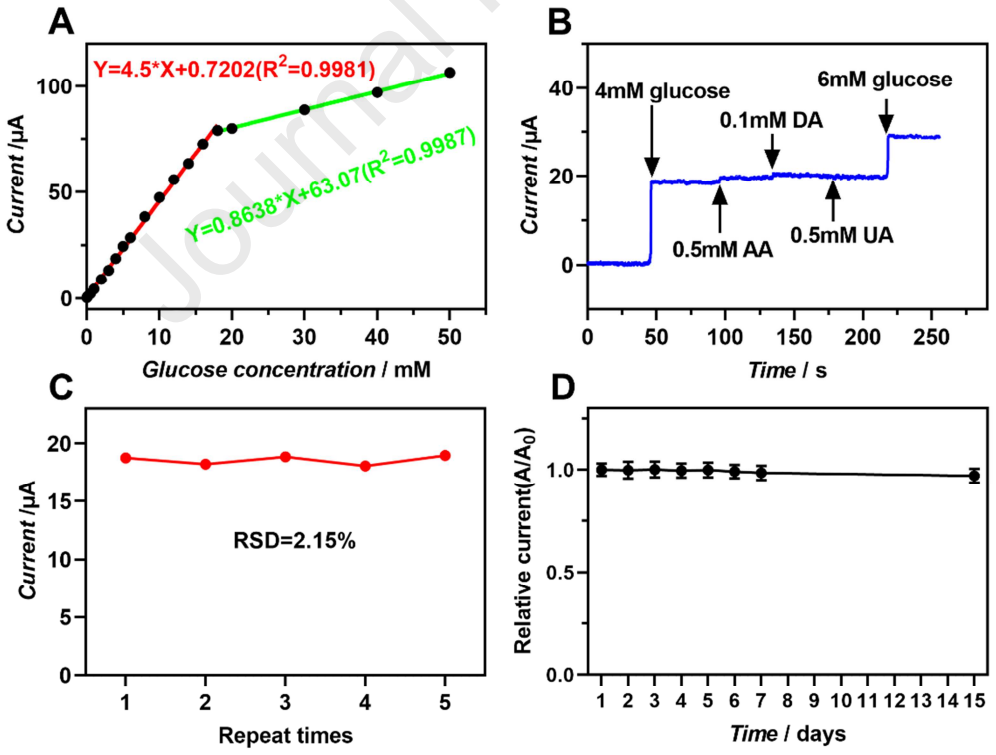

Figure. 3. A) Calibration curve of the glucose biosensor, **B)** Amperometric response recorded by the n(GOx-SFAD-PAM)/cMWCNTs/GCE-based biosensor in a stirred

solution to which 0.50 mM AA, 0.10 mM DA, and 0.5 mM UA were added, respectively; **C)** five repeated measurements for 4mM glucose of n(GOx-SFAD-PAM)/cMWCNTs/GCE-based biosensor; **D)** Results of n(GOx-SFAD-PAM)/cMWCNTs/GCE-based biosensor measuring 4mM glucose at different days. The response current obtained on the first day was treated as 100%. Data represent mean ± standard deviation (SD) from three independent experiments.

3.4. n(GOx-SFAD-PAM)-based EBFC performance

The performance of the assembled glucose/O_2 EBFC by taking the n(GOx-SFAD-PAM)/cMWCNTs/GCE as the bioanode and the bilirubin oxidase (BOD)/N-cMWCNTs/GCE as the cathode was further investigated (see details in the Supporting Information). BOD is often used as a cathodic enzyme because of its good capability of direct electronic transfer(Campbell et al., 2016). The open circuit potential ($\boldsymbol{E}^{ocp}$) reached 0.9V, as the shown curve a in **Figure. 4A.** **Figure. 4B** presents the polarization curve (a) and power density curves (b) of EBFC. For the EBFC, a maximum power density (***P***max) of 1011.21 μW cm^{-2} can be achieved at 0.378 V. The ***P***max of it is 386 times that of EBFCs constructed with native GOX/cMWCNTs/GCE (**Figure. S13**). These results indicate that n(GOx-SFAD-PAM)-based EBFC has high output power, with higher the $\boldsymbol{E}^{ocp}$ and ***P***max than reported work previously (listed in **Table S4**). Major reason might be that network containing SFAD acts as an electronic "highway" to link the electrode and the GOx active site, and accelerate electron transfer between them.

As GOx is usually easy to lose activity, lifetimes of EBFCs is relatively short (typically 8 hours to 7 days)(Moehlenbrock and Minteer, 2008). While the n(GOx-SFAD-PAM)/cMWCNTs/GCE showed desired stability, with 94% ***P***max

retaining (curve b in **Figure. S14**) after storage for 15 days. The potential value of the EBFC as a power source was also studied. Two EBFCs are connected in series, and its $\boldsymbol{E}^{ocp}$ and $\boldsymbol{P}$max reach 1.8 V and 2001.08 μW cm^{-2}, respectively, as shown curve b in **Figure. 4A** and curves b in **Figure. 4C**. A red LED could be lighted by the two EBFCs connected in series (**Figure. 4D**), suggesting a potential application of this EBFC as a power source.

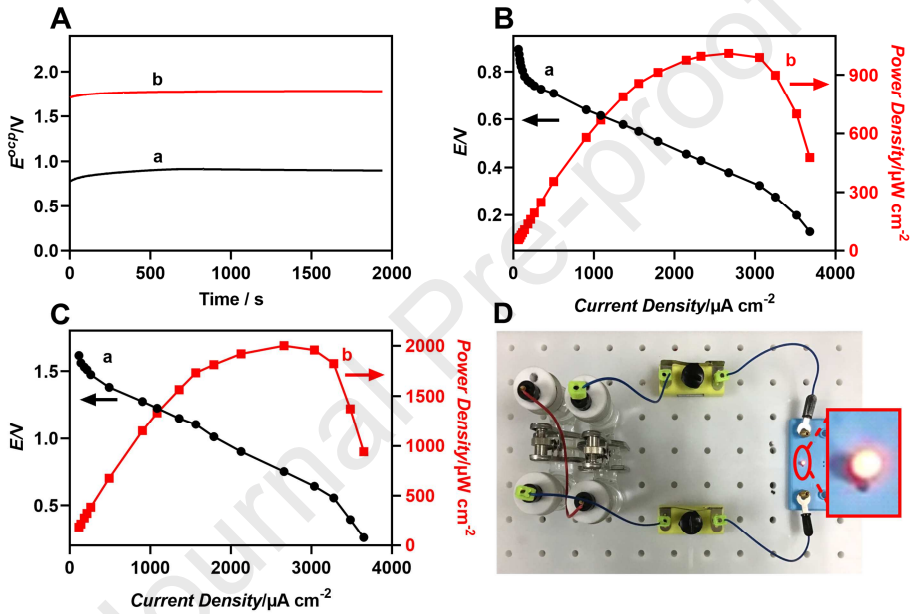

Figure. 4. A) Time course of $\boldsymbol{E}^{ocp}$ for a single EBFC (a) and for two EBFCs connected in series (b). **B)** The polarization curve (a) and power density curves (b) for a single EBFC on the first day. **C)** Polarization curves (a) and power density curves (b) of two EBFCs connected in series. **D)** A red LED was lighted by two as-prepared EBFCs connected in series.

4. Conclusions

We designed and synthesized a novel biomimetic cofactor monomer SFAD, and successfully prepared an electroactive enzyme nanocapsule n(GOx-SFAD-PAM) via in-situ polymerization. The SFAD-containing polymeric network can promote an

effective wiring of the GOx active site to electrode and significantly enhance stability of the GOx. Based on these advantages, n(GOx-SFAD-PAM)-base biosensor displays high sensitivity, good anti-interference performance and excellent stability. n(GOx-SFAD-PAM)-based EBFC has the high maximum power density (1011.21 μWcm^{-2}), which is a 386-fold increase over that of native GOx-based EBFC (2.62 μWcm^{-2}). Moreover, a red LED could be lighted by the two n(GOx-SFAD-PAM)-based EBFCs connected. This work provides a new approach for building an effective interface for transferring electrons and improving performances of enzymatic bioelectrocatalysis-based biodevices.

CRediT authorship contribution statement

Jie Huang: Data curation, Methodology, Visualization, Formal analysis, Writing - original draft. **Yuxuan Zhang:** Data curation. **Fei Ding:** Writing - review & editing. **Dong Chen:** Methodology. **Yiwen Wang:** Writing - review & editing. **Xin Jin:** Conceptualization, Methodology, Writing - review & editing, Funding acquisition, Project administration. **Xinyuan Zhu:** Supervision, Project administration, Funding acquisition.

Declaration of competing interest

The authors declare that they have no known competing financial interests or personal relationships that could have appeared to influence the work reported in this paper.

Acknowledgements

This work was financially supported by National Natural Science Foundation of China (51873106) and Shanghai Municipal Government (18JC1410800).

References

Adrian, Ruff, Julian, Szczesny, Nikola, Markovi, Felipe, Conzuelo, Sónia, Zacarias, 2018. Nat. Commun. 9, 1-10.

Arnold, H, F., 2018. Angew. Chem. Int. Ed. 57, 4143-4148.

Arnold, F.H., 2018. Angew. Chem. Int. Ed. 130, 4212-4218.

B, L.W.A., A, X.L., A, K.N., A, D., A, J.C., 2020. Biosens. Bioelectron. 165, 1-7.

Boussema, F., Gross, A.J., Hmida, F., Ayed, B., Majdoub, H., Cosnier, S., Maaref, A., Holzinger, M., 2018. Biosens. Bioelectron. 109, 20-26.

Cal, P.M.S.D., Bernardes, G.A.J.L., Gois, P.M.P., 2014. Angew. Chem. Int. Ed. 53, 10585-10587.

Campbell, A.S., Murata, H., Carmali, S., Matyjaszewski, K., Islam, M.F., Russell, A.J., 2016. Biosens. Bioelectron. 86, 446-453.

Caruana, D.J., Howorka, S., 2010. Mol. BioSyst. 6, P.1548-1556.

Chen, C., Wang, L., Tan, Y., Qin, C., Xie, F., Fu, Y., Xie, Q., Chen, J., Yao, S., 2011. Biosens. Bioelectron. 26, 2311-2316.

Chen, H., Dong, F.Y., Minteer, S.D., 2020. Nat Catal 3, 225-244.

Chen, Y., Gai, P., Zhang, J., Zhu, J., 2015. J. Mater. Chem. 3, 11511-11516.

Cheong, Hoon, Kwon, Yongmin, Ko, Dongyeeb, Shin, Minseong, Jinho, Park, 2018. Nat. Commun. 9, 1-11.

Courjean, O., Gao, F., Mano, N., 2010. Angew. Chem. Int. Ed. 121, 6011-6013.

Demin, S., Hall, E.A.H., 2009. Bioelectrochemistry 76, 19-27.

Deng, H., Teo, A.K.L., Gao, Z., 2014. Sens. Actuators, B B191, 522-528.

Dhanjai, Lu, X., Wu, L., Chen, J., Lu, Y., 2020. Anal. Chem. 92, 5830-5837.

Dong, C., Yu, H., Jiang, H., Wumaier, Y., Guo, D., Yue, S., Bai, X., Xin, J., Zhu, X., 2018. ACS Appl. Mater. Interfaces 10, 26005-26015.

Feng, G., Lucie, V., Maryse, M., Philippe, P., Nicolas, M., 2010. Nat. Protoc.

Gao, F., Viry, L., Maugey, M., Poulin, P., Mano, N., 2010. Nat. Commun. 1, 1-7.

Gao, H., Duan, H., 2015. Biosens. Bioelectron. 65, 404-419.

Güven, G., Prodanovic, R., Schwaneberg, U., 2010. Electroanalysis 22, 765-775.

Han, L., Yang, D.-P., Liu, A., 2015. Biosens. Bioelectron. 63, 145-152.

Huang J, Z.P., Jin X, Yiwen Wang, H.Y., Xinyuan Zhu, 2020. Biomater. Sci.

Huang, X., Zhang, L., Zhang, Z., Guo, S., Shang, H., Li, Y., Liu, J., 2019. Biosens. Bioelectron. 124-125, 40-52.

Jeerapan, I., Ma, N., 2019. C-J Carbon Res 5, 2-27.

Ji, Y., Gai, P., Feng, J., Wang, L., Zhang, J., Zhu, J., 2017. J. Mater. Chem. 5, 11026-11031.

Jin-Zhong, X., Jun-Jie, Z., Qiang, W., Zheng, H., Hong-Yuan, C., 2003. Chinese Journal of Chemistry 21, 1088-1091.

Kang, Z., Jiao, K., Cheng, J., Peng, R., Jiao, S., Hu, Z., 2018. Biosens. Bioelectron. 101, 60-65.

Kang, Z., Job Zhang, Y.-H.P., Zhu, Z., 2019. Biosens. Bioelectron. 132, 76-83.

Karyakin, A., A., Morozov, S., V., Voronin, O., G., Zorin, N., A., Karyakina, E., E., Fateyev, V., N., Cosnier, S., 2007. Angew. Chem. Int. Ed. 46, 7244-7246.

Kazarinov, I.A., Ignatova, A.A., Naumova, M.N., 2014. Russ. J. Electrochem. 50, 87-91.

Krikstopaitis, K., Kulys, J., Tetianec, L., 2004. Electrochemistry Communications 6, 331-336.

Li, J., Jin, X., Liu, Y., Li, F., Zhang, L., Zhu, X., Lu, Y., 2015. Chemical Communications 51, 9628-9631.

Ma, C.L., Liu, M.X., You, C., Zhu, Z.G., 2020. Bioresour. Bioprocess. 7, 1-11.

Mahadevan, A., Fernando, T., Fernando, S., 2016. Biosens. Bioelectron. 78, 477-482.

Masuda, M., Freguia, S., Wang, Y.F., Tsujimura, S., Kano, K., 2010. Bioelectrochemistry 78, 173-175.

Minteer, S.D., Milton, R.D., Hickey, D.P., Abdellaoui, S., Wu, F., 2015. Chem. Sci. 6, 4867-4875.

Moehlenbrock, M.J., Minteer, S.D., 2008. Chem. Soc. Rev. 37, 1188-1196.

Murata, H., Cummings, C.S., Koepsel, R.R., Russell, A.J., 2013. Biomacromolecules 14, 1919-1926.

Nicolas, Mano, 2019. Bioelectrochemistry 128, 218-240.

Panpan, Gai, Yusheng, Ji, Yun, Chen, Cheng, Zhu, Jianrong, Zhang, 2015. Analyst 140, 1822-1826.

Qu, F., Ma, X., Hui, Y., Chen, F., Gao, Y., 2017. Chinese Journal of Chemistry 35, 1098-1108.

Ramanavicius, A., Ryskevic, N., Kausaite-Minkstimiene, A., Bubniene, U., Baleviciute, I., Oztekin, Y., Ramanaviciene, A., 2012. Sens. Actuators, B 171-172, 753-759.

Rasmussen, M., Abdellaoui, S., Minteer, S.D., 2016. Biosens. Bioelectron. 76, 91-102.

Ruff, A., Conzuelo, F., Schuhmann, W., 2020. Nat Catal 3, 214-224.

Ruzgas, T., Tkac, J., Whittaker, J.W., 2007. Biosens. Bioelectron. 22, 1820-1824.

Sakai, T., Kumoi, T., Ishikawa, T., Nitta, T., Iida, H., 2018. Org. Biomol. Chem. 16, 3999-4007.

Scherbahn, V., Putze, M.T., Dietzel, B., Heinlein, T., Schneider, J.J., Lisdat, F., 2014. Biosens. Bioelectron. 61, 631-638.

Schwaneberg, U., Zhang, L., Cui, H., Zou, Z., Mirzaeigarakani, T., Novoa-Henriquez, C., Jooyeh, B., 2019. Angew. Chem. Int. Ed. 58, 4562-4565.

Song, R.B., Zhu, W.L., Fu, J.J., Chen, Y., Liu, L.X., Zhang, J.R., Lin, Y.H., Zhu, J.J., 2019. Adv. Mater. 32, 1903796.

Szczesny, J., Birrell, J.A., Conzuelo, F., Lubitz, W., Ruff, A., Schuhmann, W., 2020. Angew. Chem. Int. Ed. 59, 1-6.

Wang, L., Wang, Y., Qiao, Y., Wu, S., Lu, X., Zhu, J.J., Zhang, J.R., Zhou, H., 2020. Energy Environ. Sci. 13, 144-151.

Wei, W., Dong, S., Huang, G., Xie, Q., Huang, T., 2018. Sens. Actuators, B 260, 189-197.

Wei, W., Du, J., Li, J., Yan, M., Zhu, Q., Jin, X., Zhu, X., Hu, Z., Tang, Y., Lu, Y.,

2013. Adv. Mater. 25, 2212-2218.

Wong, T.S., Schwaneberg, U., 2003. Curr. Opin. Biotechnol. 14, 590-596.

Wu, F., Su, L., Yu, P., Mao, L.Q., 2017. J. Am. Chem. Soc. 139, 1565-1574.

Wu, L.X., Lu, X.B., Dhanjai, Wu, Z.S., Dong, Y.F., Wang, X.H., Zheng, S.H., Chen, J.P., 2018. Biosens. Bioelectron. 107, 69-75.

Xiao, X., Xia, H., Wu, R., Bai, L., Yan, L., Magner, E., Cosnier, S., Lojou, E., Zhu, Z., Liu, A., 2019. Chem. Rev. 119, 9509-9558.

Yan, M., Ge, J., Liu, Z., Ouyang, P., 2006. J. Am. Chem. Soc. 128, 11008-11009.

Yin, S., Jin, Z., Miyake, T., 2019. Biosens. Bioelectron. 141, 111471.

Zhang, E., Xie, Y., Ci, S., Jia, J., Wen, Z., 2016. Biosens. Bioelectron. 81, 46-53.

Zhang, Q., Song, R., Wu, Y., Lin, Z.Q., Xie, J., Tan, C.H., Loo, J.S.C., Cao, B., Zhang, J.R., Zhu, J.J., 2017a. Angew. Chem. Int. Ed. 129, 10652-10656.

Zhang, X., Chen, W., Zhu, X., Lu, Y., 2017b. ACS Appl. Mater. Interfaces 9, 7972-7978.

Zhang, X., Xu, D., Jin, X., Liu, G., Liang, S., Wang, H., Chen, W., Zhu, X., Lu, Y., 2017c. J. Controlled Release 255, 54-61.

Zhang, Z., Yu, G., Qi, L., Zheng, C., Xu, L., An, Y., Xin, J., Yang, L., Shi, L., 2018. Small 14, 1801865.

Zhao, C.E., Gai, P., Song, R., Ying, C., Zhang, J., Zhu, J.J., 2017. Chem. Soc. Rev. 46, 1545-1564.

Highlights

- To mimic the structure of glucose oxidase (GOx) cofactor (flavin adenine dinucleotide, FAD), a biomimetic cofactor containing vinyl group (SFAD) was customized.
- Electroactive GOx nanocapsules with SFAD-containing polymeric network(n(GOx-SFAD-PAM)) were synthesized via in-situ polymerization.
- SFAD containing electroactive polymeric network act as an electronic “highway” to link GOx active site to electrode, resulting in fast electron transfer as well as enhanced GOx stability
- The n(GOx-SFAD-PAM)-based biosensor has low detection potential, high sensitivity, good anti-interference performance and excellent stability.
- The n(GOx-SFAD-PAM)-based enzymatic biofuel cell yielded 385-fold greater power density compared to native one.